Earth`s Cryosphere, 2015, vol. XIX, No. 3, pp. 19–28 **http://earthcryosphere.ru/**

MODELING RECRYSTALLIZATION OF BASAL ICE IN GLACIERS

V.P. Epifanov

Ishlinskiy Institute for Problems in Mechanics, RAS,
101 Vernadsky pr., build. 1, Moscow, 119526, Russia; evp@ipmnet.ru

Mechanisms of frictional ice motion on a dry bed have been studied by means of experiments and theoretical simulation. Deformation changes in basal ice at the ice-bed interface are estimated quantitatively using an acoustic-mechanic approach. The approach consists in measuring acoustic emission and pulse-phase responses of ice subject to loading and is applied to the cases of ice flowing past an asperity and extruded through a hole. The relations between the natural resonance frequency of the source and its micro- and macroscopic properties are found using an exact analytical solution to the differential equation for an oscillator consisting of two or more particles of ice with elastic bonds between them. The stiffness of the bonds is estimated for ice of empirically known density, grain size and natural resonance frequency of mobile particles. The processes at the glacier base can be monitored remotely using acoustic spectra.

Acoustic response, amplitude-frequency spectra, glacier, modeling, ice-bed interface, frictional contact

INTRODUCTION

This work continues acoustic studies of basal ice in glaciers with implications for ice motion. Basal motion is commonly modeled in terms of friction (contact deformation of solids) [*Makkonen and Tikanmäki, 2014*] using data on ice cores or geophysical (GPR or seismic) surveys.

Few direct observations in the glaciers of Suess in Antarctica [*Sirota, 1999*], Engabereen in Northern Norway [*Cohen et al., 2006; Iverson et al., 2007*] and No. 1 in China [*Echelmeyer and Zhongxiang, 1987*] show ice motion patterns to be controlled by soft-bed deformation in a layer of ice-cemented till (cobbles, pebbles, sand, and clay) between ice at the glacier base and rock. Its properties resemble those of the intermediate layer in construction materials. This layer, produced by degradation of softer material, has its properties and structure notably different from those of the degrading solid. They are these properties that control the ultimate ice motion patterns (flow and stick-slip motion [*Iverson, 2012*]) and the flow of construction materials (purely plastic flow or that with asperity friction).

Ice motion is commonly studied in theoretical models [*Makkonen and Tikanmäki, 2014*], which predict that the layer at the ice-bed interface reduces bed friction [*Blackford et al., 2012; Pritchard et al., 2012; Sukhorukov and Loset, 2014*]. The modeling results have been validated by core studies indicating basal ice to be 1.4–2.2 times lower in effective viscosity than bulk ice and its mechanic strength increases by a factor of 1.2 [*Castelnau et al., 1996*]. The viscosity decrease was attributed either to changes in ice fabric and texture [*Alley, 1992; Wang et al., 2003; Eastgate and Sammonds, 2007*] or to bed roughness [*Wang et al., 2003*].

The thickness and density of ice are often studied by radar [*Booth et al., 2013*] or seismic methods. However, the radar (GPR) technology is yet imperfect while seismic soundings are applied rather to larger objects. The discovery of intracrystalline slip on different planes upon increasing hydrostatic pressure provided a breakthrough in understanding experimental results [*Piazolo et al., 2013*]. However, rheology research long remained focused on fitting the data to the Glen flow law [*Durham et al., 2010*] and on the physics of its constants [*Gödert and Hutter, 2000; Gillet-Chaulet et al., 2006*]. Strain-related changes to ice crystal microstructure were evaluated using neutron diffraction analysis [*Piazolo et al., 2013*], and acoustic methods were applied to monitor deformation at different scales from ice crystals to glaciers [*Epifanov, 1982; Epifanov and Glazovsky, 2010*].

These studies have provided a quantitative background for modeling the processes in basal ice, which is critical for predicting ice motion patterns. Together with the method of reduced variables extending the effective time range in experiments [*Amundson et al., 2006*], this allows reproducing long-lasting natural deformation in laboratory.

Ice motion has important implications for stability of glaciers. Predicting ice motion may be difficult due to the lack of knowledge about basal ice deformation. In this respect, modeling can furnish the required quantitative constraints under the assumption that strain accumulation across the ice-bed interface is detectable in acoustic responses. The results can be used further for setting up remote monitoring of glaciers.

The present study aims at simulating the formation of the basal ice layer and the structure of the frictional contact by estimating, with acoustic methods, of continuous strain changes in ice flowing around an asperity and extruding through a hole. The model has

Fig. 1. Ice motion in Bezenghi glacier (Northern Caucasus).

been tested in field observations of ice motion on a dry bed and of local stability of glaciers.

OBJECTS AND METHODS

Ice motion was studied in the field and in laboratory. The field experiments were performed on the Aldegondabreen glacier in Spitsbergen (with reference to data from the Bezenghi glacier in the North Caucasus, Fig. 1), as well as on the Central Tuyuksu and Molodezhny glaciers in the Northern Tien-Shan. Physical modeling was applied to samples of natural freshwater ice and frozen distilled water, at the Ishlinskiy Institute for Problems in Mechanics (Moscow).

Acoustic-mechanic approach

The integrate acoustic-mechanic approach consists in measuring acoustic emission and pulse-phase responses of ice subject to loading. The acoustic measurements provided quantitative estimates of strain changes to microstructure of ice flowing around an asperity and extruding through a hole. The changes were observed directly in ice thin sections. The instruments, methods, and data processing procedures were detailed in earlier publications [*Epifanov, 1982, 2014; Epifanov and Osokin, 2009, 2010*]. The field surveys were run using a portable acoustic line, at an operating frequency of f = 15–20 000 Hz, with a transducer fixed on a waveguide penetrating at least 750 mm into the ice (Fig. 2).

Acoustic responses of deforming ice

Acoustic monitoring of basal ice motion allows evaluating changes to the microstructure of loaded ice, reproducing bed conditions, and relating acoustic emission (AE) parameters with properties of freshwater ice [*Skudrzyk, 1971*].

1. *Effect of deformation on acoustic responses of ice.* Freshwater ice samples have been tested under compression and extension (Fig. 3, *A*, *B*, respectively), two types of stress best documented in experimental ice mechanics. Changes in strain (curves *2*, *4* in Fig. 3, *A*, *b*) correlate with those in acoustic velocity and attenuation (curves *1*, *3* in Fig. 3, *A*, *b*, *c*) and AE amplitude (Fig. 3, *A*, *a*). Attenuation (α) becomes more than three orders of magnitude greater on com-

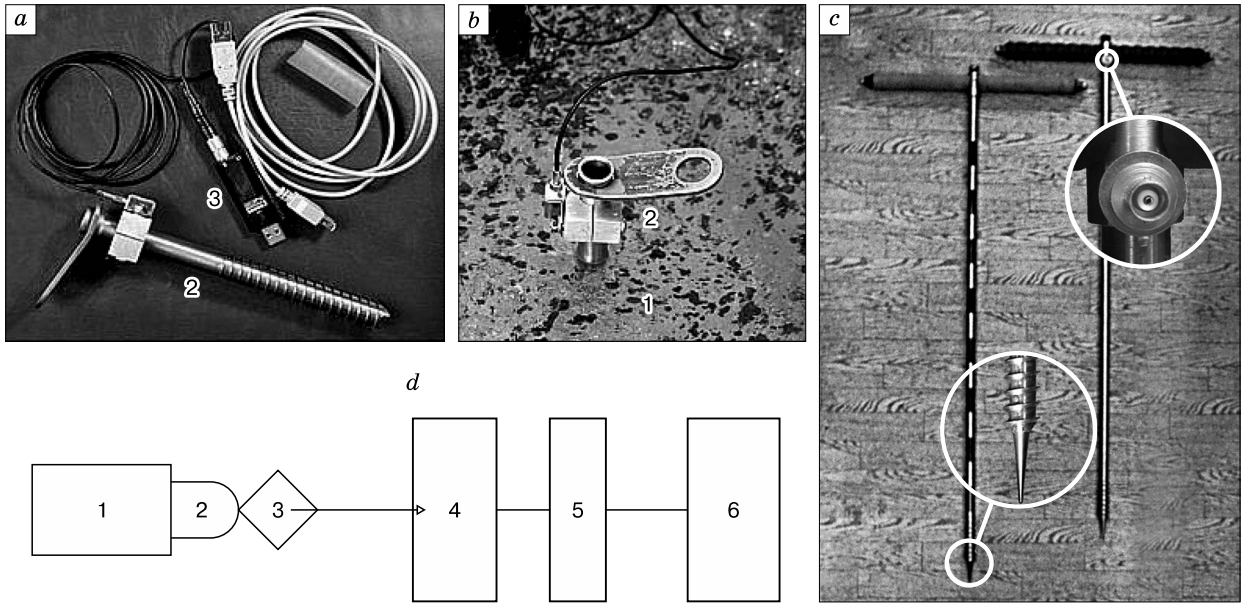

Fig. 2. Tools for field acoustic measurements in glacier ice.

a, *b*: measurement line (PC not shown): 1, 2 is waveguide with a fixed transducer, 3 is preamplifier with a power cable; *c*: waveguides. White circles mark fixing points of transducer (accelerometer) and high-frequency connector; *d*: sketch of measurement line, with waveguide (1), transducer (2), preamplifier (3), acoustic unit (4), monitor (5), and memory (6).

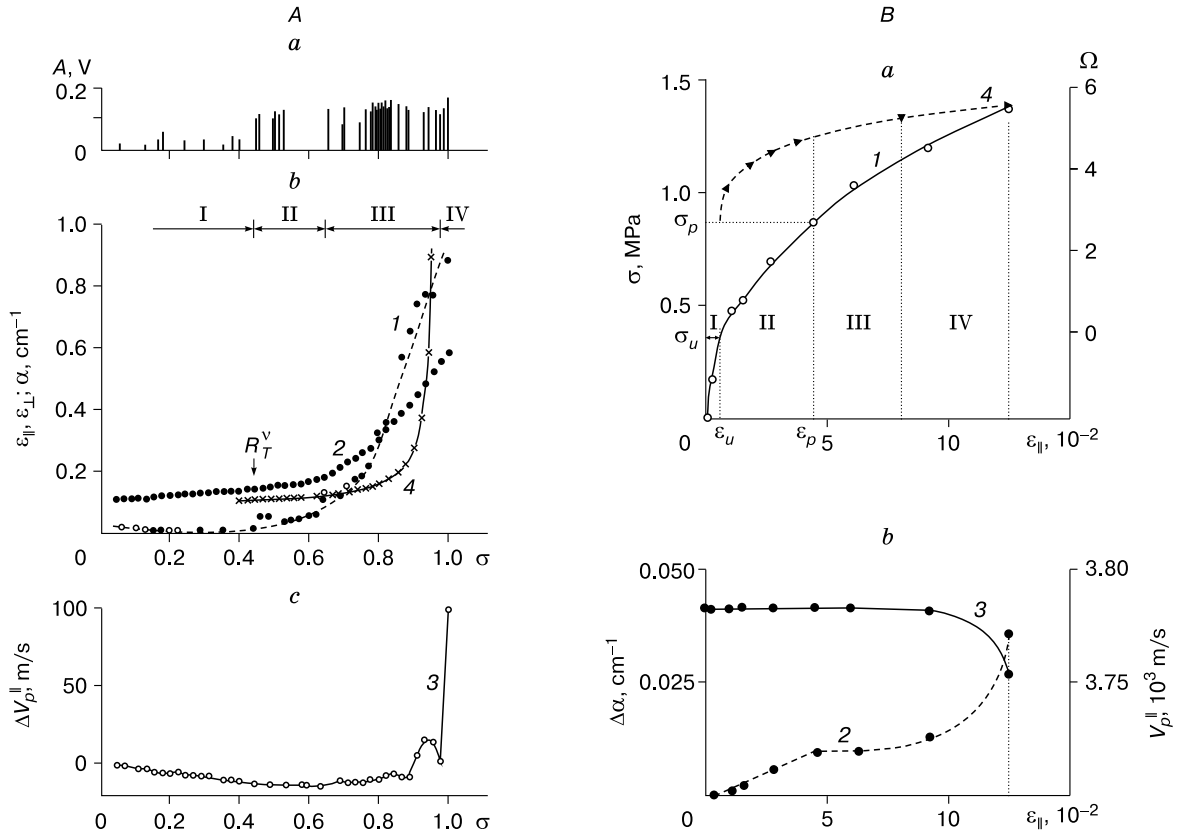

Fig. 3. Behavior of freshwater ice in compression (*A*) and extension (*B*) tests.

A: normalized stress (σ) dependences (ice temperature –40 °C) of AE amplitude (*a*), *P*-wave attenuation α (curve *1*), relative axial and lateral strain ($\varepsilon_{||}$ and $\varepsilon_{\perp}$, curves *2* and *4*, respectively) (*b*); *P* velocity decrease ($\Delta V_p^{||}$, curve *3*) (*c*); *B*: strain ($\varepsilon_{||}$) dependences (ice temperature –10 °C) of stress (σ, curve *1*) and fracture parameter ($\Omega = \Lambda L^2$, where Λ and *L* are density and length of defects, respectively, curve *4*) (*a*); attenuation increment (Δα, curve *2*) and *P* velocity ($V_p^{||}$, curve *3*) (*b*). Roman numerals are zones of elastic (I) and plastic (II–IV) deformation.

pression while wave velocity $V_p^{||}$ decreases for 30 m/s (α and $V_p^{||}$ being accurate to ±2.5 % and ±0.01 %, respectively). These changes result from accumulation of strain defects in the ice structure.

Attenuation increment under extension (curve *2* in Fig. 3, *B*) is

$$\Delta\alpha = \alpha - \alpha_0,$$

where α_0 and α are attenuation coefficients in unloaded and loaded ice, respectively.

In the same way, the velocity decrement $\Delta V_p^{||}$ (the dislocation component of ultrasonic velocity) is found from strain dependence of velocity ($V_p^{||}$, curve *3* in Fig. 3, *B*, *b*). The length *L* and concentration Λ (total length in a unit area) of dislocations are [*Truell et al., 1969*]

$$L = 1\Big/ f\left[\frac{10^6}{8.68}\frac{C}{B}\frac{\Delta\alpha}{\Delta V / V_0}\right]^{0.5},$$

$$\Lambda = 8.68\cdot 10^{-6}\left(\frac{\pi^4 B}{Gb^2}\right) f^2\left[\frac{\left(\Delta V / V_0\right)^2}{\Delta\alpha}\right], \qquad (1)$$

where *B* is the drag; *C* is the effective tension of a dislocation; *G* is the shear modulus; *b* is the magnitude of the Burgers vector. The obtained dislocation components of ultrasonic velocity ($\Delta V/V_0$) and attenuation (Δα, dB/μs) are used to calculate the parameters $\Lambda = 10^6$ m^{-2} and $L = 5\cdot 10^{-6}$ m.

Rapid increase in ultrasonic attenuation in the linear loading domain is due to transition from micro- to macro-plasticity (σ_u, ε_u are stress and strain corresponding to elastic limit) and, respectively, is accompanied by an almost 2000-fold Λ increase and a two-fold *L* increase (σ_p and ε_p are stress and strain corresponding to plastic limit). The limit stress at which the first visible fracture appears is denoted as R_T^{ν} in Fig. 3, *A*. The parameters of dislocations (microfractures) are evaluated from the dependence of ultrasonic attenuation (σ = 0.5–80 MHz) on normal-

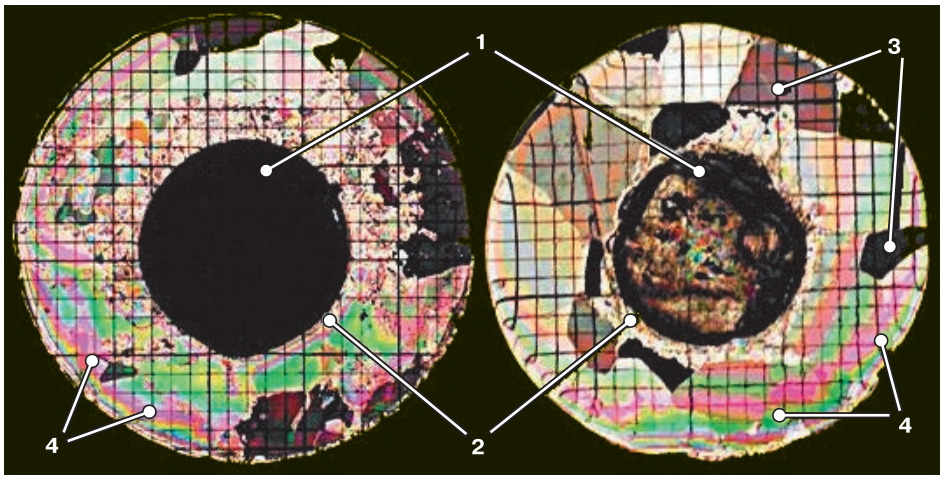

Fig. 4. Intermediate layer for different indentation depths:
1 – stamp; 2 – intermediate layer; 3 – partially deformed ice; 4 – pinnate joints.

ized scattering section of user-induced microcracks [*Epifanov, 1982*]. Structure changes with strain also can be estimated from AE spectra (to 20 kHz) using a theoretical relationship between natural resonance frequency of structure elements and acoustic compressibility [*Epifanov, 2014*].

Both extension and compression tests show that each point of strain curves has its corresponding values of acoustic parameters. Note that the empirical strain dependence of attenuation $\Delta\alpha$ (Fig. 3, *B*, *b*) fits the classic division into domains of elastic (σ_u, ε_u) and plastic (σ_p, ε_p) deformation (Fig. 3, *B*, *a*). The domains of elastic (I) and plastic (II–IV) deformation in smooth strain curves are detectable from sharp acoustic changes. Changes in deforming ice are expressed quantitatively via the parameter Ω that refers to accumulation of defects [*Epifanov, 2004*].

Thus, acoustic measurements are applicable to evaluate changes in ice deforming under loading.

2. *Ice-bed interface*. Ice deformation must cause the greatest changes at contact with obstacles (asperities) which are commonly present on the bed and act as stress concentrators. Deformation across the ice-bed interface was simulated by indentation of a circular stamp into an ice plate. The interface layer (2 in Fig. 4) appears in thin sections of freshwater ice samples cut across the long axis of the stamp (1 in Fig. 4). It forms immediately on the stamp surface by recrystallization and consists of round ice crystals (3 in Fig. 4) about two orders of magnitude smaller than the initial grain diameters ($\overline{D}$ ~ 0.2–0.3 mm against $\overline{D}$ ~ 15–20 mm). The faces of the initial crystals remain angular, and the interface layer looks like a tube with 1.5 mm thick walls. Its apparent local thickening is due to cracks (pinnate joints) producing color bands (4 in Fig. 4) and to pre-fracture zones in the ice matrix (Fig. 5) [*Epifanov and Yur'ev, 2006*].

The AE spectra correlate well with the stages of plastic deformation, and hence with the mechanisms of fracture in freshwater ice (Fig. 6). AE responses of ice to stamp indentation have peaks on transition from static friction to sliding (Fig. 6). Peaks, as markers of the transition from viscoplastic shear to stick-slip (slider block) motion, rise above continuous acoustic emission of low amplitude and frequency. The reason is that the stick-slip mechanism includes basal creep, which is of small scale relative to the motion of blocks.

Fig. 5. Deformation upon quasi-static indentation:
1 – pinnate joints; 2 – ice sample (140 × 140 × 140 mm).

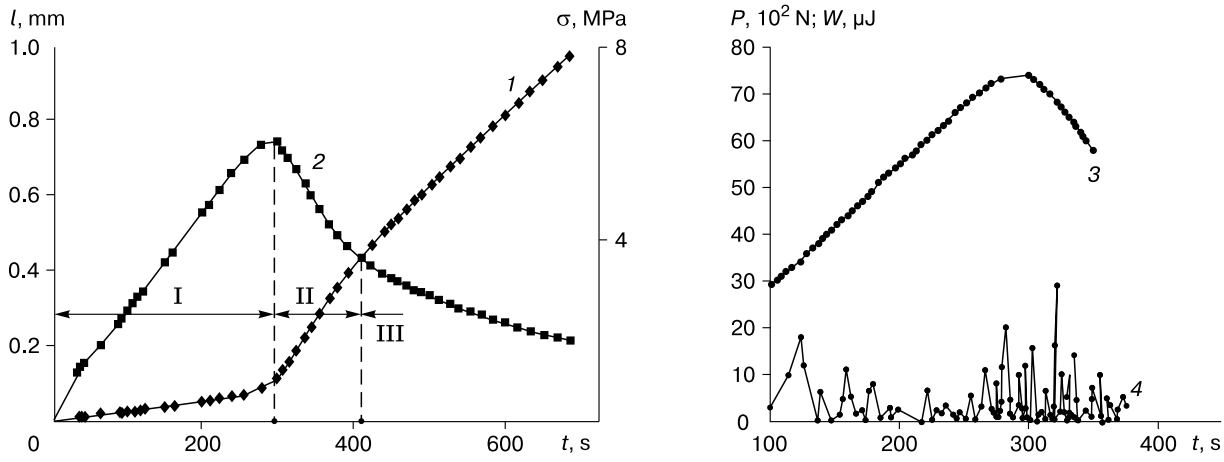

Fig. 6. Time (*t*) dependences of indenter displacement (*l*) (*1*), shear stress σ (I–III are shear stages) (*2*), axial force *P* (*3*), AE energy (*W*) (*4*).

The deformation style changes depending on the loading conditions (strain rate and temperature) and indenter (stamp) diameter: at a strain rate of ~0.001 s^{-1} and a temperature of –11 °C, the deformed ice molten from the surface becomes extruded if the indenter is less than 6 mm but forms a column with pinnate joints if the indenter diameter exceeds 6 mm.

The interface ice layer has high yield. At shearing stages II and III, its effective elastic moduli are two or even three orders of magnitude less than the initial elastic shear modulus (72 and 1 MPa at stages II and III, respectively, against 3.5 GPa). They are even lower than those inferred from strain dependence because the latter misses dissipative friction losses.

The generalized empirical D/h dependence of maximum stress obtained from experiments with indenters of different diameters D and ice plates of different thicknesses h is valid for real objects of several meters in size.

Note that the deforming ice-bed interface is orders of magnitude thicker than a similar layer in metals. This basic difference is apparently due to a high homologous temperature and a particular structure of ice crystals. The mechanic properties of the interface were investigated using measurements by specially designed methods.

3. *Ice flow experiments*. Ice extrusion through a hole is a first-approximation model of glacier-bed interaction. In confined conditions (uniform compression), slip occurs on lattice planes other than basal ones, which changes ice rheology. Polycrystalline ice becomes as plastic as to flow over the bed already at a shear stress of $\sigma_\tau \approx 47$ kPa [*Goldsby and Kohlstedt, 2001; Gow and Veesse, 2007; Hammann et al., 2007*].

As shown in the previous experiment, the formation of a highly yielding ice structure is due to joint action of normal σ_n and shear σ_τ stresses. Mylonitization at the bed contact (a substrate in the model and rocks in nature) was studied in ice extrusion experiments using a pressure cell (Fig. 7). The cell consists of a cylindrical shell, 50 mm in diameter, with a flat bottom and a lid attached to the case. Through a screw hole in the bottom, a high-pressure fitting is attached and water is injected into the cell. There is a cone in the lid opening into a 10 mm wide and 25 mm long channel with a valve (a ~2 mm thick flexible copper membrane). High pressure in the cell is created either by freezing distilled water or by air pumping through the fitting under a manometer control. After being filled with distilled water, the cell is shut tightly and placed in a cryostat at –34 °C. The water freezing and ice flow processes are monitored, respectively, by pulse-phase and AE measurements or visually.

Ice extrusion through a hole requires a stress of 12.6 MPa [*Bell, 1973*], which is controlled by hole diameter, temperature, etc., rather than being a material constant. The extruding ice changes in micro-

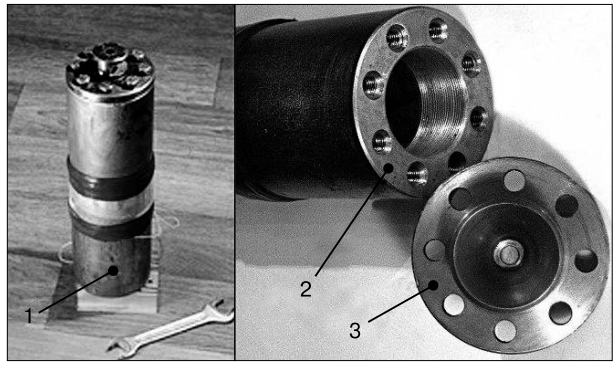

Fig. 7. Pressure cell.
1 – assembly, 2 – shell, 3 – lid.

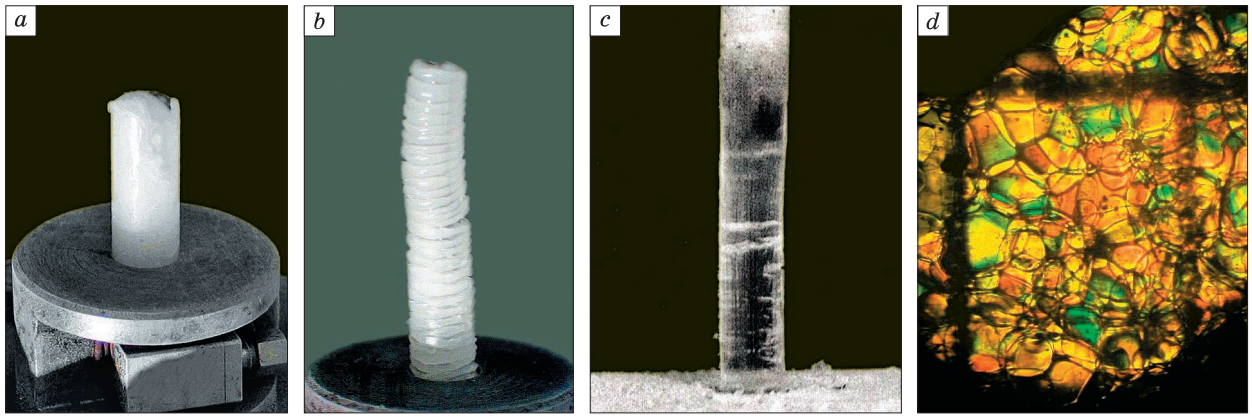

Fig. 8. Ice extrusion though holes of different diameters.

a, *b*: diameter 10 mm; *c*: diameter 8 mm; *d*: ice structure in column (grid size 0.2 mm).

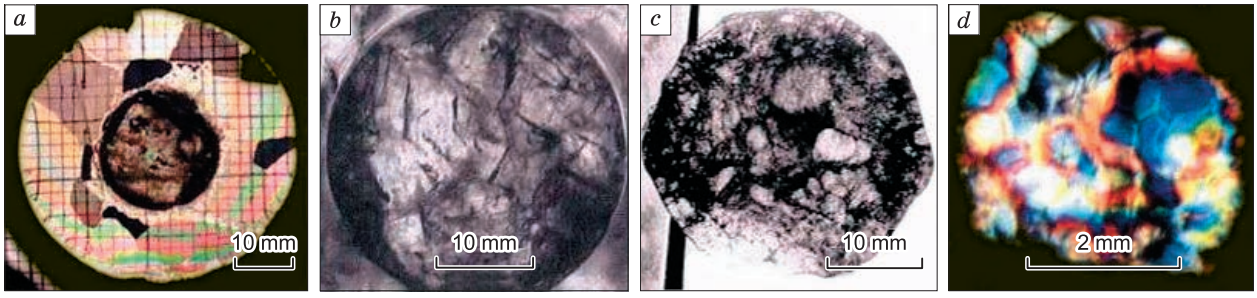

Fig. 9. Deformation of freshwater ice samples.

a: initial structure; *b*, *c*: recrystallization; *d*: ice structure in column.

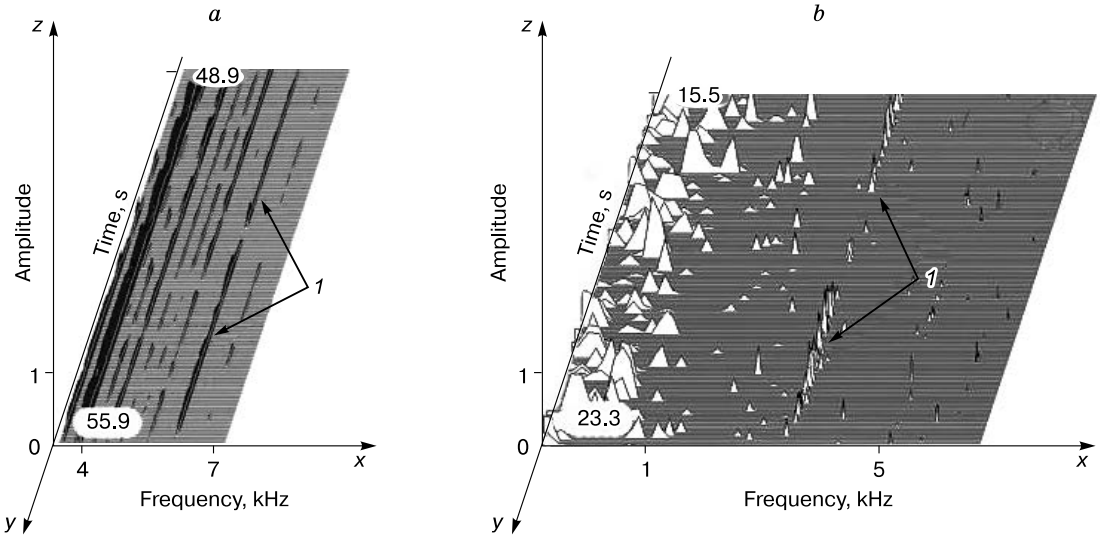

Fig. 10. Acoustic emission spectra.

a: ice extrusion through a hole; *b*: ice motion in Aldegondabreen glacier; *1* "dash-line" pattern in a response to adhesion fracture.

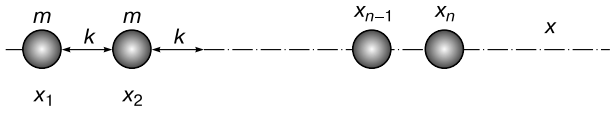

Fig. 11. Model of oscillators.

structure and acoustic properties. For instance, at a flow rate of 0.64 mm/min (~300 m/yr), *P* velocity ($V_p^{\parallel}$) in ice (average density 883 kg/m^3 at –17 °C) increases from 3862 m/s to 3889 ± 6 m/s (Fig. 8, *c*). The ~27 m/s velocity increase corresponds to a notable increase in dynamic modulus and hence in strength of ice, which is consistent with the results reported by *Gillet-Chaulet et al.* [*2006*]. However, ice looses its transparency already after an hour of flow through the channel. Similar effects of fracture and partial loss of transparency were often reported for ice cores. A goffered column (Fig. 8, *b*) results from stick-slip motion of ice along the contact surface, possibly, due to change from dry to lubricated friction and the respective change in the external to internal friction ratio.

The evolution of ice deformation (Fig. 9) records a transition from stick-slip motion (Fig. 9, *b*, *c*) to flow along the bed (Fig. 9, *d*). The visual difference in ice microstructure correlates with difference in values of acoustic and rheological parameters (e.g., about two orders of magnitude for effective shear modulus and ~ 27 m/s for *P* velocities). It exceeds the measurement error and thus represents structure changes in deforming basal ice measurable both in the field and in laboratory.

Stick-slip motion of ice along the channel is accompanied by elastic pulses, looking like dash lines in AE spectra (Fig. 10, *a*), with their amplitude and frequency controlled by adhesion and fracture extent. Similar responses were recorded at 1 to 5 kHz in the Aldegondabreen (Spitsbergen) and Central Tuyuksu glaciers (Fig. 10, *b*).

Compared with "dash lines" obtained by modeling, those for natural glaciers are shifted toward low frequencies, for several reasons: different source parameters, long distances traveled by acoustic waves in glaciers and, consequently, greater attenuation at higher frequencies. Generally, the AE spectra agreement between friction tests and measurements in glaciers confirm the possibility of using acoustic data for monitoring ice deformation. Inasmuch as the acoustic wavelengths exceed the crystal size, scattering is small, ice is supposed to be homogeneous and isotropic while the thermoelastic effect is vanishing. These assumptions allow analyzing the spectra in linear approximation.

4. ***Relation between ice crystal microstructure and macroscopic properties.*** The elastic and inertial properties of ice can be related using a harmonic oscillator model (Fig. 11):

Table 1. **Exact formulas for natural frequencies (ω_n) of oscillators**

n	ω_1	ω_2	ω_3	ω_4	ω_5
2	0	$\sqrt{\frac{2k}{m}}$			
3	0	$\sqrt{\frac{k}{m}}$	$\sqrt{\frac{2k}{m}}$		
4	0	$\sqrt{\left(2-\sqrt{2}\right)\frac{k}{m}}$	$\sqrt{\frac{2k}{m}}$	$\sqrt{\left(2+\sqrt{2}\right)\frac{k}{m}}$	
5	0	$\sqrt{\left(3-\sqrt{5}\right)\frac{k}{2m}}$	$\sqrt{\frac{k}{m}}$	$\sqrt{\left(3+\sqrt{5}\right)\frac{k}{2m}}$	$2\sqrt{\frac{k}{m}}$

$$\ddot{x} + \omega^2 x = 0, \qquad (2)$$

where x is the displacement; $\ddot{x}$ is the second time derivative (acceleration); ω is the angular frequency. At the natural frequency $\omega_0 = 2\pi f_0$, the exact solution to the differential equation can be used for two oscillators consisting of *n* (two or more) identical material points with the same mass *m*, linked via elastic bonds of the same stiffness *k* (Table 1).

The added mass of material point is $m = 4\pi R^3\rho$, where *R* is the oscillator radius in m (for mobile ice particles); ρ is the ice density, kg/m^3. The stiffness k_2 for an oscillator comprising two material points (Table 1) is

$$k_2 = 16\pi^3 f^2 R^3 \rho\,. \qquad (3)$$

Similar equations apply to oscillators with *n* points. The exact number of particles producing the acoustic pulse being unknown, the elasticity corresponding to the observed spectra fragments is found from known ice microstructure parameters for different *n* (Fig. 10, *a*). Specifically, at the radius of particles $1\cdot10^{-4}$ m and the ice density 883 kg/m^3, for 5.94 and 11.3 kHz, the stiffness values (*k*) are obtained as functions of the number of mobile particles in the oscillator (Fig. 12). Note that for *n* = 3 and the reso-

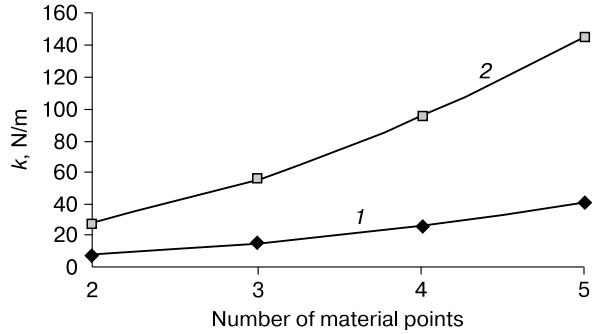

Fig. 12. Theoretical elasticity vs. number of material points for 5.94 kHz (*1*) and 11.3 kHz (*2*).

nance frequencies 5.94 and 11.3 kHz, k can be found as 15.4 and 55.9 N/m, respectively.

The values found by the acoustic method agree with the constants 15.5 and 56.0 N/m that represent stretching and bending of the O–H–O and H–O–H bonds at 273 K obtained by NMR [*Zimmerman and Pimental, 1962*].

DISCUSSION

Motion is the principal characteristic of a glacier as a mass of mostly meteoric ice. The previous ice motion studies focused more on the yield stress for freshwater ice and its viscosity in axial compression tests. However, the ice thermodynamics in these experiments differs markedly from the state of basal ice in glaciers. The motion of a natural glacier along its bed can be simulated in terms of confined frictional ice-bed interaction.

In the case of dry friction, the deformation of basal ice is given by

$$\frac{d\sigma}{dt} = G\frac{d\varepsilon}{dt} - G\frac{\sigma}{\eta} = G\left(\frac{d\varepsilon}{dt} - \frac{\sigma}{\eta}\right), \qquad (4)$$

where $d\varepsilon/dt$ is the strain rate; η is the viscosity; σ/η is the ice creep rate; G is the shear modulus. As follows from (4), deformation can occur either as creep at $d\varepsilon/dt < \sigma/\eta$ or as stick-slip motion at $d\varepsilon/dt > \sigma/\eta$. Simple mathematical models of glaciers are limited by vanishing curvatures of their bed and top surfaces. The rheology of basal ice depends on many thermodynamic factors, including the normal-to-shear stress ratio. Extrusion was used as a way to model boundary conditions at the bed.

On the other hand, stress buildup at $d\varepsilon/dt > \sigma/\eta$ makes the ice discontinuous, and the forming kinematic couplings lead to stick-slip motion (Fig. 9, *b*, *c*). This motion corresponds to the descending branch of strain curves (the region of supercritical strain in Fig. 6). The point of local stability loss and the kinetics of fracture growth show up in acoustic responses [*Epifanov and Glazovsky, 2010*].

Being distant sources, glaciers produce AE responses with low frequency and amplitude (Fig. 9, *b*). This is consistent with the facts that (i) the calculated distance to the acoustic source is commensurate with the ice thickness and (ii) the acoustic spectra of glaciers are similar to the respective spectra of physical models. Namely, the acoustic spectra of glaciers contain periodic pulses and phase shifts as "dash-line" features at 1.2 and 2.6 kHz. Such patterns within the range 4–10 kHz were observed in experiments and originated from fracture at the friction contact (Fig. 9, *b*). Correspondingly, the acoustic spectra of glaciers must record fracture during stick-slip motion on a rough bed.

The transition from static to sliding friction is a local stability loss (Fig. 6). The stability loss point correlates with changes in the AE responses (frequency, amplitude, peak width) and effective elasticity of ice. Adhesive and cohesive fracture modes have latent times (~0.06 s and 0.8–1.0 s, respectively) which correspond to certain AE parameters.

Normal stress at the ice-bed frictional contact causes polygonization of super-stressed crystals, which diminish in size and loose preferred orientations. Friction heat can cause melting and maintain recrystallization by regelation. If pressure at grain boundaries is high enough (>10 MPa), the crystal fragments melt from the surface and become rounded (Fig. 9). Joint action of these factors gives rise to a new fabric consisting of finely crushed ice and ice cement (mylonite). All these processes at the ice-bed friction contact create conditions for the formation of a 1.5 mm thick intermediate layer.

Cataclastic deformation of ice and its changes during flow, especially, on extrusion through a hole, produce 5 mm high "columns" of transparent ice, at a temperature above –10 °C and a pressure of ~15 MPa (Fig. 8, *c*, *d*). Such ice has a fine granular structure and is highly plastic, which allows the columns to remain transparent and keep shape for a while despite large residual stress. As the water freezing conditions in the pressure cell change, ice entraps small air bubbles and becomes opaque (Fig. 8, *a*). Goffered columns of extruded ice form when the exterior pressure exceeds the interior one (Fig. 9, *b*). The diversity of ice microstructures (Fig. 9) and the changes to column surfaces (paratectonic recrystallization, cataclasis, and extrusion) are similar to patterns of blue bands, friction breccias, etc., commonly observed in natural glaciers.

According to laboratory physical modeling of stress metamorphism in ice samples, basal ice in most of glaciers must be fine-grained. Indeed, such ice was found in Antarctic ice cores. Thus, physical modeling can simulate prolonged natural processes in permafrost. Time-scale consistency [*Paterson, 1994*] poses no problems in such experiments: Modeling recrystallization and laterally confined deformation of glacier ice (motion along slip planes or grain boundaries) takes just a few hours. The reported results allow outlining approaches to prediction of ice motion patterns as prerequisites for acoustic monitoring of glaciers.

CONCLUSIONS

Defects in deforming polycrystalline freshwater ice subject to loading can be estimated from acoustic responses at high and low frequencies: from 500 kHz to 100 MHz (pulsed responses) and from 100 Hz to 20 kHz (acoustic emission). AE spectra are recorded synchronously with small-amplitude ultrasonic pulse ($\leq 5 \cdot 10^4$ Pa) records, and the acoustic parameters (frequency, amplitude and waveform of signals, as well as attenuation and velocity of waves) are correlated to strain and stress.

Acoustic responses of deforming ice measured over the whole range of stresses, till fracture, place more rigorous constraints on the elastic and plastic limits and have implications for parameters of dislocations. The mechanic and structural ice properties correlate with accumulation of micro- and macroscopic dislocations.

Rapid recrystallization produces an intermediate layer at the ice-bed interface, orders of magnitude thicker than a similar layer in construction materials (~1.5 mm against ~0.0001 mm). This basal ice is fine-crystalline, with ~0.2 mm round gains, and it flows at 0.64 mm/min. Changes to the ice crystal microstructure and motion patterns can be monitored from acoustic emission.

Oscillations generated at the ice-bed frictional contact have been analyzed in terms of a linear model, tested against the known bond constants for water molecules. The obtained first-approximation consistency for two model material points makes the model applicable to physical modeling and suitable for explaining the acoustic spectra of glaciers. The reason is that the model material point and the stiffness of its bonds with other points are used in chain models in continuum mechanics.

The microscale patterns of ice deformation and fracture revealed in the laboratory tests remain valid for large natural ice masses. Namely, samples up to a few meters in size show similar shifts in the low-frequency acoustic spectra. The correlation between the fracture scattering section and the acoustic parameters measured by the pulse-phase and AE methods likewise holds for the meter scale.

The experiments confirm the possibility for deep recrystallization associated with short-term ice creep under laterally confined shear. Thus, laboratory physical modeling can simulate very slow natural permafrost processes in a reasonably short time.

This line of research appears to be promising and important, both in theoretical and applied aspects. The developed methods and instruments are suitable for performing the research objectives. The results can be used for monitoring of basal ice in glaciers and ice fracture at obstacles.

I wish to thank academician V.F. Zhuravlev for his interest to the study, discussions, and valuable advice.

The study was supported by grant 15-05-07767_a from the Russian Foundation for Basic Research.

References

Alley, R.B., 1992. Flow-law hypotheses for ice-sheet modeling. J. Glaciol. 38 (129), 245–256.

Amundson, J.M., Truffer, M., Luthi, M.P., 2006. Time-dependent basal stress conditions beneath Black Rapids Glacier, Alaska, USA, inferred from measurements of ice deformation and surface motion. J. Glaciol. 52 (178), 347–357.

Bell, J.F., 1973. Experimental Foundations of Solid Mechanics, in: Truesdell, C. (Ed.), Mechanics of Solids, Vol. I, Springer, New York, 813 pp.

Blackford, J.R., Skouvaklis, G., Purser, M., Koutsos, V., 2012. Friction on ice: stick and slip. Faraday Discussion, 243–254, doi:10.1039/C2FD00128D.

Booth, A.D., Mercer, A., Clark, R., Murray, T., Jansson, P., Axtell, Ch., 2013. A comparison of seismic and radar methods to establish the thickness and density of glacier snow cover. Ann. Glaciol. 54 (64), 73–82, doi:10.3189/2013AoG64A044.

Castelnau, O., Duval, P., Lebensohn, R.A., Canova, G., 1996. Viscoplastic modeling of texture development in polycrystalline ice with a self-consistent approach: Comparison with bound estimates. J. Geophys. Res. 101, 13851–13868.

Cohen, D., Hooyer, T.S., Iverson, N.R., Thomason, J.F., Jackson, M., 2006. Role of transient water pressure in quarrying: A subglacial experiment using acoustic emissions. J. Geophys. Res. 111, 2003–2012, doi:10.1029/2005JF000439.

Durham, W.B., Prieto-Ballestros, O., Goldsby, D.L., Kargel, J.S., 2010. Rheological and thermal properties of ice materials. Space Sci. Rev. 153 (1), 273–298, doi:10.1007/s11214-009-9619-1.

Eastgate, T., Sammonds, P., 2007. Fabric and textural evolution within the EPICA ice cores: EDC and EDML. Geophys. Res. Abstr. 9, 02761.

Echelmeyer, K., Zhongxiang, W., 1987. Direct observations of basal sliding and deformation of basal drift at sub-freezing temperatures. J. Glaciol. 33 (113), 83–98.

Epifanov, V.P., 1982. Fracture of polycrystalline ice. Dokl. RAN 267 (6), 1364–1367.

Epifanov, V.P., 2004. Elasticity of polycrystalline ice. Materialy Gliatsiol. Issled. 96, 101–111.

Epifanov, V.P., 2014. Acoustics application for snow cover study. Earth's Cryosphere (Kriosfera Zemli) XVIII (3), 92–103.

Epifanov, V.P., Glazovsky, A.F., 2010. Acoustic characteristics as an indicator of the specifics of ice movement in glaciers. Kriosfera Zemli XIV (4), 42–55.

Epifanov, V.P., Osokin, N.I., 2009. Plastic flow and tensile strength of snow cover on mountain slopes of Spitzbergen Island. Kriosfera Zemli XIII (2), 82–93.

Epifanov, V.P., Osokin, N.I., 2010. Study of strength properties of snow cover on the mountain slope, Spitsbergen archipelago. Kriosfera Zemli XIV (1), 81–91.

Epifanov, V.P., Yur'ev, R.V., 2006. Fracture viscosity of fresh ice. Doklady Physics 51 (1), 28–32.

Gillet-Chaulet, F., Gagliardini, O., Meyssonnier, J., Zwinger, T., Ruokolainen, J., 2006. Flow-induced anisotropy in polar ice and related ice-sheet flow modeling. J. Non-Newtonian Fluid Mech. 134, 33–43.

Gödert, G., Hutter, K., 2000. Material update procedure for planar transient flow of ice with evolving anisotropy. Ann. Glaciol. 30, 107–114.

Goldsby, D.L., Kohlstedt, D.L., 2001. Superplastic deformation of ice: Experimental observation. J. Geophys. Res. 106 (B6), 11017–11030.

Gow, A.J., Veesse, D., 2007. Physical properties, crystalline textures and *c*-axis fabrics of the Siple Dome (Antarctica) ice core. J. Glaciol. 53 (183), 573–584.

Hammann, L., Weikuat, C., Azuma, N., Kipfstuhl, S., 2007. Evolution of ice crystal microstructure during creep experiments. J. Glaciol. 53 (182), 479–589.

Iverson, N.R., 2012. A theory of glacial quarrying for landscape evolution models. Geology 40, 679–682.

Iverson, N.R., Hooyer, T.S., Fischer, U.H., Cohen, D., Moore, P.L., Jackson, M., Lappegard, G., Kohler, J., 2007. Soft-bed experiments beneath Engabreen, Norway: regelation infiltration, basal slip and bed deformation. J. Glaciol. 53 (182), 323–340.

Makkonen, L., Tikanmäki, M., 2014. Modelling the friction of ice. Cold Regions Sci. Technol. 84–93, doi:10.1016/j.coldregions. 2014.03.002.

Paterson, W.S.B., 1994. The Physics of Glaciers. Elsevier, Oxford, New York, Tokyo, 480 pp.

Piazolo, S., Wilson, C.J.L., Luzin, V., Brouzet, C., Peternell, M., 2013. Dynamics of ice mass deformation: Linking processes to rheology, texture, and microstructure. Geochem. Geophys. Geosystems 14 (10), 4185–4194.

Pritchard, R.S., Knoke, G.S., Echert, D.C., 2012. Sliding friction of sea ice blocks. Cold Regions Sci. Technol. 76–77, 8–16.

Sirota, P., 1999. Direct Observations of Basal Sliding and Deformation of Basal Drift at Sub-Freezing Temperatures. Ph.D., University of Otago, New Zealand, 92 pp.

Skudrzyk, E.J., 1971. The Foundations of Acoustics: Basic Mathematics and Basic Acoustics. Springer-Verlag, Science, Berlin, 790 pp.

Sukhorukov, S., Loset, S., 2014. Friction of sea ice on sea ice. Cold Regions Sci. Technol. 102, 84–93.

Truell, R., Elbaum, C., Chick, C.B., 1969. Ultrasonic Methods in Solid State Physics, Diagrams. Academic Press, New York, 464 pp.

Wang, Y., Kipfstuhl, S., Azuma, N., Thorsteinsso, T., Miller, H., 2003. Ice-fabrics study in the upper 1500 m of the Dome C (East Antarctica) deep ice core. Ann. Glaciol. 37, 97–104.

Zimmerman, R., Pimental, G.C., 1962. The infrared spectrum of ice; temperature dependence of the hydrogen bond potential function, in: MacMillan, N.Y. (Ed.), Advances in Molecular Spectroscopy, Pergamon, Oxford, 2, pp. 726–737.

Received October 30, 2014